EJN European Journal of Neuroscience

FENS Federation of European Neuroscience Societies

European Journal of Neuroscience, Vol. 39, pp. 1720–1728, 2014 doi:10.1111/ejn.12476

A highly sensitive fluorescent indicator dye for calcium imaging of neural activity *in vitro* and *in vivo*

Mayumi Tada, Atsuya Takeuchi, Miki Hashizume,* Kazuo Kitamura and Masanobu Kano
Department of Neurophysiology, Graduate School of Medicine, The University of Tokyo, 7-3-1 Hongo, Bunkyo-ku, Tokyo, 113-0033, Japan

Keywords: cerebellum, mouse, neocortex, population activity, two-photon imaging

Abstract

Calcium imaging of individual neurons is widely used for monitoring their activity *in vitro* and *in vivo*. Synthetic fluorescent calcium indicator dyes are commonly used, but the resulting calcium signals sometimes suffer from a low signal-to-noise ratio (SNR). Therefore, it is difficult to detect signals caused by single action potentials (APs) particularly from neurons *in vivo*. Here we showed that a recently developed calcium indicator dye, Cal-520, is sufficiently sensitive to reliably detect single APs both *in vitro* and *in vivo*. In neocortical neurons, calcium signals were linearly correlated with the number of APs, and the SNR was > 6 for *in vitro* slice preparations and > 1.6 for *in vivo* anesthetised mice. In cerebellar Purkinje cells, dendritic calcium transients evoked by climbing fiber inputs were clearly observed in anesthetised mice with a high SNR and fast decay time. These characteristics of Cal-520 are a great advantage over those of Oregon Green BAPTA-1, the most commonly used calcium indicator dye, for monitoring the activity of individual neurons both *in vitro* and *in vivo*.

Introduction

The activity of individual neurons induces calcium influx through voltage-dependent calcium channels, which can be monitored by using calcium indicator dyes. For the past few decades, various calcium indicators have been developed that have enabled the analysis of intracellular calcium dynamics (Grynkiewicz *et al.*, 1985; Regehr *et al.*, 1989; Miyakawa *et al.*, 1992; Eilers *et al.*, 1995; Yuste & Denk, 1995; Svoboda *et al.*, 1996; Finch & Augustine, 1998; Yasuda *et al.*, 2004). Furthermore, these dyes can be used in combination with two-photon microscopy to monitor the activity of neuronal populations *in vivo* (Stosiek *et al.*, 2003; Ohki *et al.*, 2005; Kerr *et al.*, 2007; Sato *et al.*, 2007; Sohya *et al.*, 2007; Ozden *et al.*, 2009; Schultz *et al.*, 2009; Rochefort *et al.*, 2011). Therefore, synthetic fluorescent calcium indicators have been a powerful tool to uncover the function of neural circuit dynamics and its underlying mechanisms in the intact brain from single synapse to single cell resolution (see, for review: Grewe & Helmchen, 2009; Grienberger & Konnerth, 2012).

Conventional synthetic calcium indicators can reliably resolve single action potentials (APs) and individual synaptic inputs in single neurons by perfusing the dye through an intracellular recording pipette in both brain slices and intact animals (Svoboda *et al.*, 1997; Waters *et al.*, 2003; Jia *et al.*, 2010; Chen *et al.*, 2011; Takahashi *et al.*, 2012). However, bolus loading of membrane-permeable calcium indicators (acetoxymethyl ester derivatives of fluorescent indicators) (Tsien, 1981) has the great advantage that the activity of hundreds of neurons can be monitored simultaneously (Yuste & Katz, 1991; Stosiek *et al.*, 2003). Although this method is sufficiently sensitive to detect single APs in both acute slices and organotypic slice cultures (Ikegaya *et al.*, 2005; Yuste *et al.*, 2011), the signal-to-noise ratio (SNR) is apparently lower *in vivo* such that single APs are often difficult to detect (Sato *et al.*, 2007; Golshani *et al.*, 2009) (but see Kerr *et al.*, 2005; Grewe *et al.*, 2010), presumably due to the scattering of fluorescence signals by thick brain tissues. This limitation is critical particularly for monitoring the activity of neurons with a low firing rate.

In this report, we demonstrate that a new BAPTA-based fluorescent calcium indicator, Cal-520, yields calcium transients with large amplitudes and high SNR in neocortical pyramidal cells and cerebellar Purkinje cells, which are sufficient to detect single APs reliably in the intact brain.

Materials and methods

The care of animals and experimental procedures were carried out in accordance with national and institutional guidelines, and all experimental protocols were approved by the Animal Experimental Committee of the University of Tokyo.

Animal surgery for in vivo *imaging*

The C57BL6/J male mice (postnatal days 28–61) were anesthetised by intraperitoneal injection of 1.9 mg/g urethane (for neocortical

Correspondences: Masanobu Kano and Kazuo Kitamura, as above.
E-mails: mkano-tky@m.u-tokyo.ac.jp and kkitamura@m.u-tokyo.ac.jp

**Present address*: Department of Biochemistry, Faculty of Medicine, Saitama Medical University, 38 Morohongo, Moroyama-machi, Iruma-gun, Saitama 350-0495, Japan

Received 11 October 2013, revised 5 December 2013, accepted 6 December 2013

imaging), or 100 mg/kg ketamine and 10 mg/kg xylazine (for cerebellar imaging). The depth of anesthesia was monitored regularly by observing whisker movements and the pinch withdrawal reflex of the hindlimb; additional doses of anesthetic were given as needed. Body temperature was kept at 37 °C with a heating pad (FHC, Bowdoin, ME, USA). The mouse was fixed on a custom stereotaxic apparatus under a surgical microscope (Leica). A skin incision was made along the midline and the skull was partly exposed. A stainless steel frame was glued to the skull with superglue and dental cement. A small craniotomy (~2 mm in diameter) was made to expose the left barrel cortex (3 mm lateral to the midline and 1.5 mm caudal to the bregma) or the left Crus IIa of the cerebellum (4 mm lateral and 2 mm posterior to the occipital bone line) using a high-speed drill (ULTIMATE500; NSK, Kanuma, Tochigi, Japan). The dura was carefully removed, and the craniotomy was filled with 1.5% agarose (type IIIa, Sigma-Aldrich) in a solution of the following composition (in mM): 150 NaCl, 2.5 KCl, 10 HEPES, 2 $CaCl_2$, 1 $MgCl_2$, pH 7.3. A coverslip was placed over the agarose to minimise brain movements. The mouse was then transferred to the animal stage under the two-photon microscope.

Dye injection

Multi-cell bolus loading of calcium indicator dye was performed as described previously (Stosiek *et al.*, 2003; Sullivan *et al.*, 2005; Mukamel *et al.*, 2009; Ozden *et al.*, 2009; Schultz *et al.*, 2009; Hashizume *et al.*, 2013). Cal-520 acetoxymethyl ester (Cal-520 AM) (AAT Bioquest, Sunnyvale, CA, USA; excitation/emission wavelength, 492/514 nm; spectra available on manufacturer's website, www.aatbio.com; K_d, 320 nM; quantum yield, 0.75) or Oregon Green 488 BAPTA-1 acetoxymethyl ester (OGB-1 AM) (Invitrogen) was dissolved with 20% (for neocortical neurons) or 10% (for cerebellar Purkinje cells) w/v Pluronic F-127 (Invitrogen) in dimethyl sulfoxide. The dye aliquot was then diluted with the extracellular solution containing Alexa 594 fluorescent dye (20 μM; Invitrogen). The final concentration of the calcium indicator dye was 1 and 0.2 mM for neocortical and cerebellar neurons, respectively. The dye solution was sonicated for 1 min, filtered with a 0.2 μm syringe filter to remove dye aggregation, and then transferred to a glass pipette (2–7 MΩ).

Dye ejection was performed in layer 2/3 of the barrel cortex (200–300 μm from the surface) or in the cerebellar molecular layer (50–60 μm from the surface) at 5 psi for 3 min using Picospritzer (Parker Hannifin, Hollis, NH, USA). Successful dye ejection was monitored by two-photon imaging on the Alexa channel. When the pipette tip was clogged up during dye ejection, brief pulses of higher pressure (10–20 psi) were applied to recover the flow of dye from the tip of the pipette. Calcium imaging was performed more than 30 min after dye ejection.

In vivo *two-photon microscopy*

In vivo calcium imaging was performed by using a custom-built two-photon microscope (MOM, Sutter Instrument, Novato, CA, USA) controlled by ScanImage software (Pologruto *et al.*, 2003). The brain was illuminated with a pulsed Ti:sapphire laser (MaiTai HP, 800–830 nm wavelength, 80 MHz repetition rate, 100 fs pulse width; NewPort Spectra-Physics, Santa Clara, CA, USA). The laser was focused through a 40 × water-immersion objective lens (LUMPLFL/IR40XW, Olympus) onto the tissue. The average laser power was adjusted to be < 15 mW at the specimen. Fluorescence signals of Cal-520 or Oregon Green 488 BAPTA-1 (OGB-1) and Alexa 594 were divided into green and red channels, respectively, by a dichroic mirror and emission filters (Chroma, Bellows Falls, VT, USA), and were detected by a pair of photomultiplier tubes (Hamamatsu, Shizuoka, Japan).

To obtain calcium transients from neuronal populations, images were acquired at a resolution of 128 × 128 pixels (sampling rate, ~8 Hz) for ~2 min. These image stacks were analysed offline. For high-speed imaging of calcium transients in bolus-loaded specimens, linescan (sampling rate, 500 Hz) was performed on somata of the cortical neurons or on dendrites of cerebellar Purkinje cells.

Simultaneous calcium imaging and loose-seal cell-attached recordings in vivo

A glass electrode (5–7 MΩ) filled with the extracellular solution containing Alexa 594 (50 μM) was inserted into the barrel cortex or cerebellar cortex and targeted to a soma that had been loaded with OGB-1 AM or Cal-520 AM. At about 10 min after the establishment of the cell-attached configuration, simultaneous loose-seal cell-attached recording and linescan calcium imaging (500 Hz) were performed on the soma of cortical neurons or on the dendrites of Purkinje cells at ~100 μm from the soma. The electrophysiological data were filtered at 10 kHz and digitised at 20 kHz by using Multiclamp 700B and Digidata 1322A (Molecular Devices, Sunnyvale, CA, USA), and acquired by AxoGraph X (AxoGraph Scientific, Sydney, Australia).

Preparation of neocortical slices

The 3–4-week-old C57BL6/J male mice were killed under CO_2 anesthesia by cervical dislocation followed by decapitation. Whole brains were immediately removed in ice-cold oxygenated (95% O_2 and 5% CO_2) artificial cerebrospinal fluid containing (in mM): 125 NaCl, 2.5 KCl, 1.25 NaH_2PO_4, 26 $NaHCO_3$, 2 $CaCl_2$, 1 $MgCl_2$, and 25 glucose. Acute coronal brain slices containing the barrel cortex (250–300 μm thick) were prepared using a vibrating microtome (VT1200S; Leica). Slices were incubated for at least 30 min in oxygenated artificial cerebrospinal fluid at 30 °C and later stored at room temperature (23–25 °C) before transferring them to the recording chamber under the two-photon microscope.

Simultaneous whole-cell recordings and calcium imaging in vitro

Brain slices were mounted in the immersion-type recording chamber under the two-photon microscope and continuously perfused with oxygenated artificial cerebrospinal fluid at 30 °C during recordings. Individual layer 2/3 pyramidal neurons in the barrel cortex were visualised by detecting forward scattered infrared laser light with the transmitted light detector of the two-photon microscope (Wimmer *et al.*, 2004). Patch pipettes were pulled from borosilicate glass capillaries on a vertical puller (PC-10; Narishige, Tokyo, Japan). The resistance of the patch pipette ranged from 4 to 8 MΩ when filled with the intracellular solution containing (in mM): 133 K-$MeSO_3$, 7.4 KCl, 10 HEPES, 3 Na_2ATP, 0.3 Na_2GTP, 0.3 $MgCl_2$, 0.05 Alexa 594, and either 0.1 Cal-520 potassium salt (AAT Bioquest) or 0.1 OGB-1 potassium salt (Invitrogen). Whole-cell current-clamp recordings were performed using an EPC10 amplifier (Heka Elektronik, Lambrecht, Rhineland-Palatinate, Germany), filtered at 10 kHz and digitised at 20 kHz. Calcium imaging was started at least 30 min after break-in to allow diffusion of the dye into the cell.

A laser scanning two-photon microscope (FV1000-MPE; Olympus) equipped with a pulsed laser (MaiTai HP DeepSee; NewPort Spectra-Physics) was used for two-photon calcium imaging with a

water-immersion objective lens (LUMPLFL/IR40XW, Olympus). The fluorescence signals of Cal-520 or OGB-1 and Alexa 594 were separated into green and red channels, respectively, and detected by a pair of photomultiplier tubes (Hamamatsu). Simultaneous whole-cell recording and linescan calcium imaging (714 Hz) were conducted on the soma of the pyramidal cells. APs were triggered by current injections (0.8 nA, 2 ms) through the patch pipette. Each trial was repeated at least 10 times and the mean value is presented.

Data analysis

All imaging and electrophysiological data were analysed using ImageJ (http://rsb.info.nih.gov/ij/), Igor Pro (WaveMetrics, Lake Oswego, OR, USA), MATLAB (MathWorks, Natick, MA, USA), and AxoGraph X. For population calcium imaging in the barrel cortex, regions of interest corresponding to individual neuronal somata were automatically defined by using the pixel correlation method (Smith & Häusser, 2010). The fluorescence signals of all of the pixels in each region of interest were averaged and calcium transients were detected by using a simple thresholding method.

For simultaneous calcium imaging and cell-attached recordings, detection of calcium transients was triggered by the onset of APs (for cortical neurons) or complex spikes (for cerebellar Purkinje cells) measured in the electrophysiological recording. Fluorescence signals in the linescan data were averaged over the entire width of the soma and dendrite. Calcium transients were calculated as $\Delta F/F = (F-F_0)/(F_0-F_b)$, where F_0 is baseline fluorescence and F_b is background fluorescence for Cal-520 or OGB-1. The peak amplitude of calcium transients was defined as the difference between the baseline (average $\Delta F/F$ of 40 ms before the onset of APs or complex spikes) and the average of five data points around the peak. The SNR was calculated as the peak amplitude of calcium transients divided by the SD of the baseline fluctuation of the fluorescence trace. The calcium transient traces were smoothed with a sliding window of three to five points for presentation. The statistical significance of the data was tested by a two-sided Welch two-sample *t*-test unless otherwise noted, and all tests were performed using R (http://www.r-project.org/). All of the data are presented as mean ± SEM.

Results

Imaging of calcium transients evoked by action potentials in neocortical pyramidal cells in vitro

Calcium transients in response to APs were recorded in neocortical pyramidal cells in acute brain slices to quantify the signal amplitude and SNR. We first compared calcium signals detected by Cal-520 with those detected by OGB-1, a commonly used fluorescent indicator, which has a similar K_d value (Cal-520, 320 nM; OGB-1, 170 nM). Pyramidal cells in the barrel cortex were whole-cell patch-clamped and APs were evoked by injecting depolarising current pulses. Either Cal-520 or OGB-1 was loaded through a patch pipette and spike-induced calcium transients were assessed by high-speed linescan imaging (sampling rate, 714 Hz) (Fig. 1A). With the number of evoked APs used (one, two, four and eight APs at 20 Hz), the amplitude of calcium transients increased in a linear fashion in both Cal-520- and OGB-1-loaded pyramidal cells (Fig. 1B and C). Cal-520 showed a significantly higher amplitude and SNRs of calcium transients in all numbers of APs tested (Fig. 1C and D). It is of note that a single AP induced calcium transients with a larger amplitude (0.702 ± 0.140 ΔF/F for Cal-520 and 0.129 ± 0.030 ΔF/F for OGB-1; seven cells in five mice and seven cells in four mice, respectively, $P = 0.006$) and SNR (6.630 ± 0.668 for Cal-520 and 4.323 ± 0.522 for OGB-1, $P = 0.019$) in Cal-520-loaded cells, which enables the reliable detection of single APs. Although there was no statistical difference in the kinetic dynamics of both indicators (10–90 rise time: 0.0637 ± 0.0045 and 0.0854 ± 0.0314 s; seven cells in five mice and seven cells in four mice, respectively, $P = 0.518$; decay time constants: 0.691 ± 0.113 s for Cal-520 and 2.114 ± 0.955 s for OGB-1, $P = 0.188$) (Fig. 1E), these results show the superior sensitivity of Cal-520 over OGB-1 for the detection of calcium transients. The improved sensitivity of Cal-520 enabled the detection of discrete calcium transients induced by spike trains of higher frequencies up to 10 Hz (Fig. 1F).

Imaging of calcium transients evoked by action potentials in neocortical neurons in vivo

Multi-cell bolus loading of the acetoxymethyl ester derivative of the indicator dye was performed to monitor the population activity of neurons in the barrel cortex (Stosiek *et al.*, 2003; Golshani *et al.*, 2009). Cal-520 AM or OGB-1 AM was injected into layer 2/3 of the mouse barrel cortex (200–300 μm from the surface). At about 30 min after dye loading, Cal-520 or OGB-1 was penetrated into the neurons and glia. Spontaneous calcium transients in multiple neurons in the field of view were reliably detected using Cal-520 (Fig. 2A and B) as well as OGB-1 (Fig. 2C). The mean frequency of spontaneous calcium transients was indistinguishable between Cal-520 and OGB-1 (0.0458 ± 0.002 and 0.0410 ± 0.0022 Hz; 171 cells in 12 mice and 12 cells in four mice, respectively, $P = 0.64$, Mann–Whitney *U*-test) (Fig. 2D). The average number of active neurons in a field of view of the Cal-520-filled cortex (147 × 147 μm), which showed at least one spontaneous AP in 2 min, was significantly larger than that of the OGB-1-filled cortex (7.77 ± 0.27 and 1.71 ± 0.14 cells/field of view, 12 and four mice, respectively, $P = 0.0002$, Mann–Whitney *U*-test) (Fig. 2E). This result reflects the fact that Cal-520-filled cells showed a larger amplitude of calcium transients than OGB-1-filled cells (0.318 ± 0.001 and 0.218 ± 0.008 $\Delta F/F$, 171 cells in 12 mice and 12 cells in four mice, respectively, $P = 0.03$, Mann–Whitney *U*-test) (Fig. 2F), and thus the mean SNR of individual calcium transients by Cal-520 was significantly higher than that by OGB-1 (14.62 ± 0.04 and 8.65 ± 0.28, $P = 0.0002$, Mann–Whitney *U*-test) (Fig. 2G). Calcium transients evoked by sensory stimulation to contralateral whiskers were also clearly observed in multiple neurons (Fig. 3).

To quantitatively compare the signal amplitude and SNR, we next performed high-speed linescan imaging (sampling rate, 500 Hz) (Fig. 4A and B). The mean amplitude of individual calcium transients using Cal-520 was significantly larger than that using OGB-1 (0.696 ± 0.010 and 0.434 ± 0.011 $\Delta F/F$, 49 cells in nine mice and 14 cells in four mice, respectively, $P = 0.02$, Mann–Whitney *U*-test) (Fig. 4C), which resulted in higher SNRs (5.390 ± 0.052 for Cal-520 and 3.465 ± 0.077 for OGB-1, $P = 0.0004$) (Fig. 4D). The kinetic properties of calcium transients were not different between Cal-520 and OGB-1 [10–90 rise time (Fig. 4E): 0.053 ± 0.001 and 0.099 ± 0.006 s, 49 cells in nine mice and 14 cells in four mice, respectively, $P = 0.09$; decay time constants by double-exponential fitting (Fig. 4F): 0.755 ± 0.009 and 1.055 ± 0.010 s for Cal-520 (46 cells in nine mice), 0.675 ± 0.037 and 1.196 ± 0.043 s for OGB-1 (12 cells in four mice), $P = 0.60$ and 0.28, respectively].

As both the mean amplitude and mean SNR for each calcium transient, which we quantified above (Figs 2F and G, and 4C and D), included different numbers of APs/transient, further quantification was required to compare the true performance of these indica-

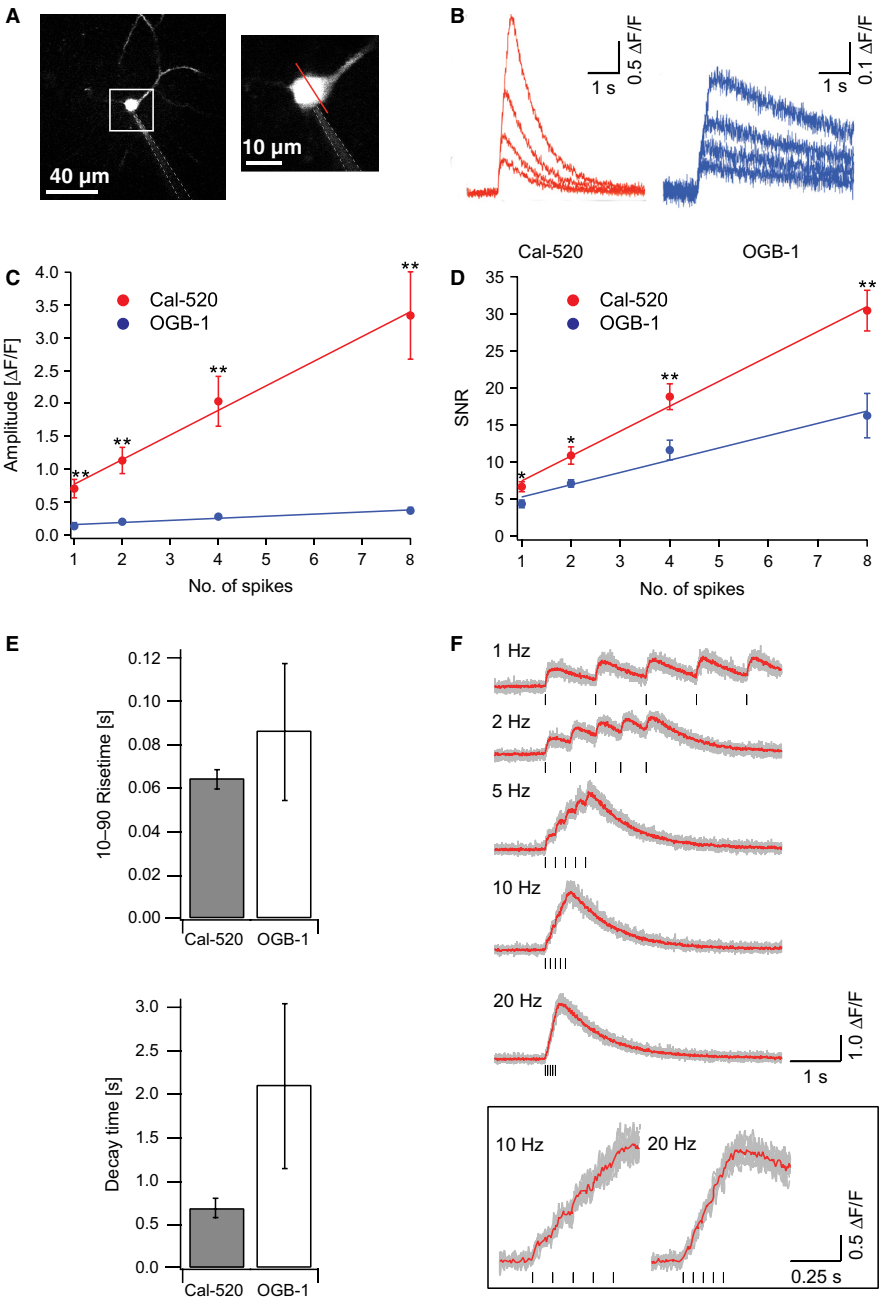

FIG. 1. Properties of Cal-520 examined in layer 2/3 pyramidal cells in the barrel cortex in acute brain slices. (A) Representative image of whole-cell patch-clamp recording from a pyramidal cell in the barrel cortex. Dashed lines indicate the patch pipette. A magnified image is shown in the right panel. The red line indicates the position of the linescan. (B) Representative traces of fluorescence response ($\Delta F/F$) of Cal-520 and OGB-1 in response to one, two, four, and eight spike trains at 20 Hz. Mean amplitude (C) and SNR (D) of Cal-520 and OGB-1 in response to one to eight spike trains at 20 Hz. Error bars indicate SEM (n = 7 cells each, $^*P < 0.05$, $^{**}P < 0.01$). (E) Rise times and decay time constants of calcium transients induced by single APs. Error bars indicate SEM (n = 7 cells each). (F) Trial-averaged fluorescence transients of Cal-520 to five spike trains at different frequencies. Bottom: responses to 10 and 20 Hz spike trains are shown in an expanded time scale. Gray lines indicate individual sweeps (n = 10). Red thick lines indicate average traces. Stimuli are indicated by the black vertical lines.

tors. Therefore, we performed simultaneous loose-seal cell-attached recordings and high-speed linescan imaging to clarify the relationship between the calcium transients and APs (Fig. 5A). The amplitude of the calcium transients linearly correlated with the number of APs (Fig. 5B), and the amplitude of calcium transients per spike, which was calculated as the peak amplitude divided by the number of APs, was significantly larger for Cal-520 than for OGB-1 (0.188 ± 0.008 and 0.052 ± 0.009 $\Delta F/F$, nine and four cells, respectively, $P = 0.0008$) (Fig. 5C). The SNR per spike was also superior for Cal-520 (1.69 ± 0.08 and 0.54 ± 0.04, nine and four cells, respectively, $P = 0.002$) (Fig. 5D). It is notable that Cal-520 could clearly detect calcium signals evoked by single APs, which were barely detectable using OGB-1 (Fig. 5E).

The time course of the change in fluorescence signals by Cal-520 was examined. The mean baseline fluorescence, amplitude, and frequency of spontaneous calcium transients in neurons were compared at different time points during imaging (Fig. 6). During 1–4 h after the injection, Cal-520 showed no significant change in the mean amplitude

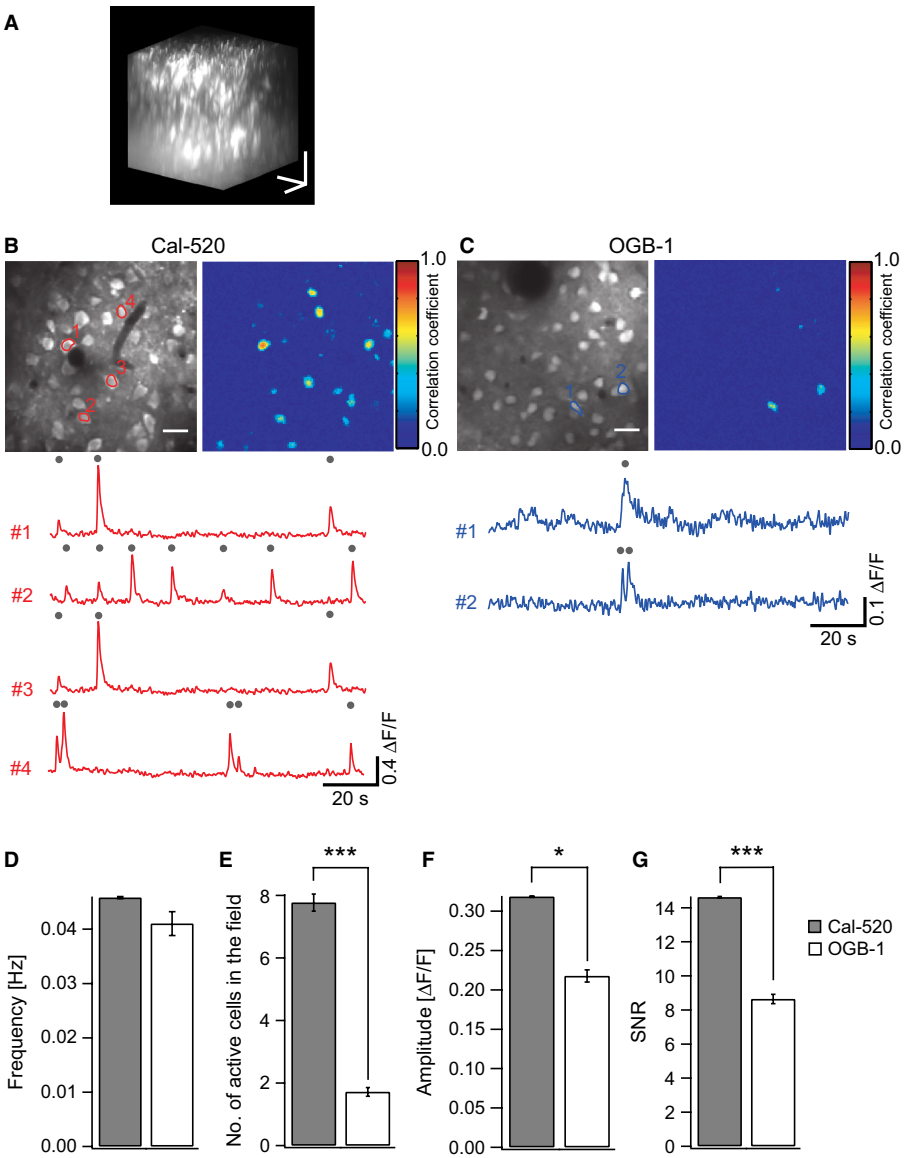

FIG. 2. *In vivo* two-photon calcium imaging of layer 2/3 neurons in the barrel cortex labeled by multi-cell bolus loading of Cal-520 AM or OGB-1 AM. (A) Three-dimensional projection image of Cal-520 AM-loaded barrel cortex. Depth, 80–250 μm from pia. Scale bars, 50 μm. Neurons in layer 2/3 of the left barrel cortex labeled with Cal-520 AM (B) or OGB-1 AM (C). Upper left: representative images of the field of view (FOV) showing the somata of labeled neurons. Upper right: neurons producing calcium transients were automatically detected by the pixel correlation method and are shown in the color map. Lower: representative traces of calcium transients from corresponding regions of interest shown in the upper left panels, which were defined as the area showing a higher correlation coefficient than the predetermined threshold. Gray dots indicate calcium transients detected from the baseline noise. Scale bars, 20 μm. (D–G) Bar graphs showing the frequency of APs (D) and number of active cells per FOV (E), amplitude of calcium transients (F), and SNR (G) by multi-cell bolus loading of Cal-520 (filled columns, n = 171 cells in 12 mice) or OGB-1 (open columns, n = 12 cells in four mice). *P < 0.05, ***P < 0.001. Error bars indicate SEM.

of calcium transients (0.325 ± 0.003 and 0.291 ± 0.009 ΔF/F, P = 0.49, t-test) (Fig. 6C), despite an increase of baseline fluorescence intensity (52.8 ± 0.3 and 73.9 ± 0.8 F in 59 cells and 22 cells, respectively, P = 0.00002, t-test) (Fig. 6B). The frequency of spontaneous calcium transients was also unchanged (0.0457 ± 0.0006 and 0.0391 ± 0.011 Hz, P = 0.36, t-test) (Fig. 6D).

Imaging of calcium transients evoked by climbing fiber input in cerebellar Purkinje cells in vivo

We next compared calcium transients measured with Cal-520 with those measured with OGB-1 in cerebellar Purkinje cells *in vivo*. In the cerebellar cortex, spontaneous calcium transients in Purkinje cell dendrites have been shown to be triggered by complex spikes evoked by climbing fiber inputs (Ozden *et al.*, 2009; Schultz *et al.*, 2009; Kitamura & Häusser, 2011). Cal-520 AM or OGB-1 AM was bolus loaded into the cerebellar molecular layer of the cerebellar cortex (Mukamel *et al.*, 2009; Ozden *et al.*, 2009; Schultz *et al.*, 2009; Hashizume *et al.*, 2013). Cal-520 or OGB-1 was penetrated into various cell types, including Purkinje cells, molecular layer interneurons and Bergmann glia. The somata of Purkinje cells in the Purkinje cell layer (Fig. 7A, upper) and their dendrites extending along the rostrocaudal axis in the molecular layer (Fig. 7A, lower) were clearly labeled with both Cal-520 (Fig. 7A, left) and OGB-1 (Fig. 7A, right).

High-speed linescan imaging was performed on dendrites of the bolus-loaded Purkinje cells to analyse the properties of calcium transients (five cells in four mice for Cal-520 and six cells in two mice for OGB-1) (Fig. 7B and C). The mean amplitude of the calcium

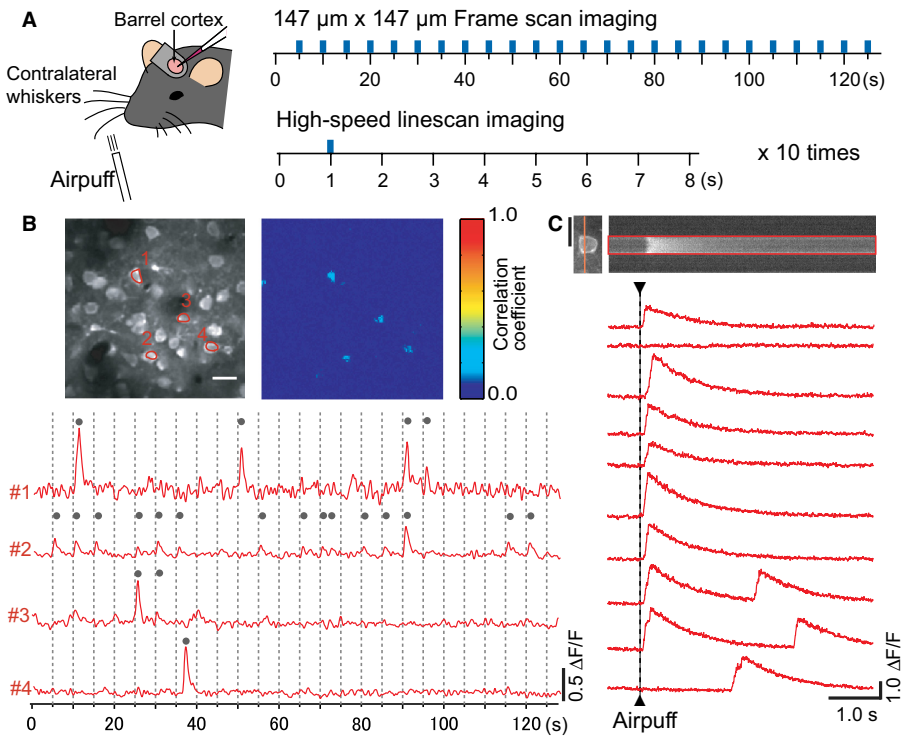

FIG. 3. Sensory-evoked calcium transients in neocortical neurons labeled with Cal-520. (A) Configuration of the experiment. Brief airpuff stimuli (40 psi, 50 ms) were delivered to the contralateral whiskers while neuronal activities in the left barrel cortex were recorded. In frame scan imaging, stimuli (blue bars) were delivered at 5 s intervals during an imaging session of 125 s. In linescan imaging, stimulus was delivered every 8 s. (B) Sensory-evoked calcium transients in multiple neurons. Upper: the fluorescence changes in neurons were recorded while aifpuff stimuli were delivered. Lower: representative traces of calcium transients from four regions of interest (#1–#4) shown in the upper left panel. Vertical broken lines indicate airpuff stimulation. Gray dots indicate calcium transients detected from the baseline noise. (C) Sensory-evoked calcium transients recorded with high-speed linescan imaging. Upper left: representative image showing the pyramidal cell labeled with Cal-520. Upper right: a scanned image (2 ms/line) recorded at the position indicated by the orange line in the upper left panel. Lower: calcium transients recorded in the cell shown above. Eight of 10 airpuff stimuli evoked calcium transients. Scale bars, 20 μm.

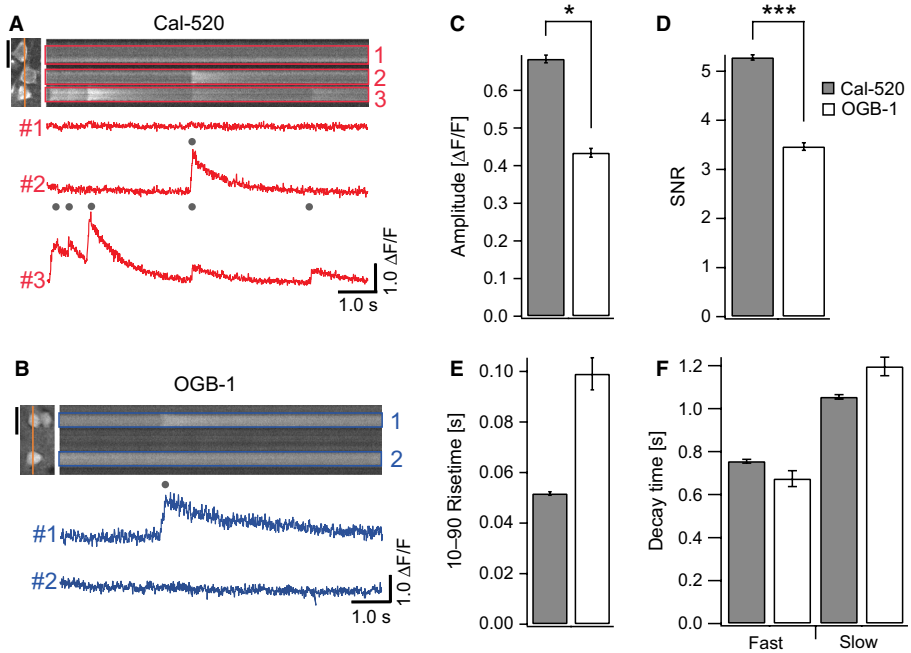

FIG. 4. Properties of calcium transients in neocortical neurons *in vivo* measured with Cal-520 and OGB-1. Representative linescan imaging from somata of layer 2/3 neurons labeled with Cal-520 (A) or OGB-1 (B). Scale bars, 20 μm. Upper right: linescan images obtained at the position indicated by the orange lines in the upper left panels. Lower: spontaneous calcium transients recorded at the regions of interest shown as the rectangles in the upper right panels. Gray dots indicate calcium transients detected from the baseline noise. (C–F) Bar graphs showing the properties of calcium transients measured with Cal-520 (filled columns) or OGB-1 (open columns). Cal-520 showed higher mean amplitude of calcium transients than OGB-1 (C), resulting in higher SNR (D). Rise times (E) and decay time constants (F) of calcium transients were indistinguishable between Cal-520 and OGB-1. $*P < 0.05$, $***P < 0.001$.

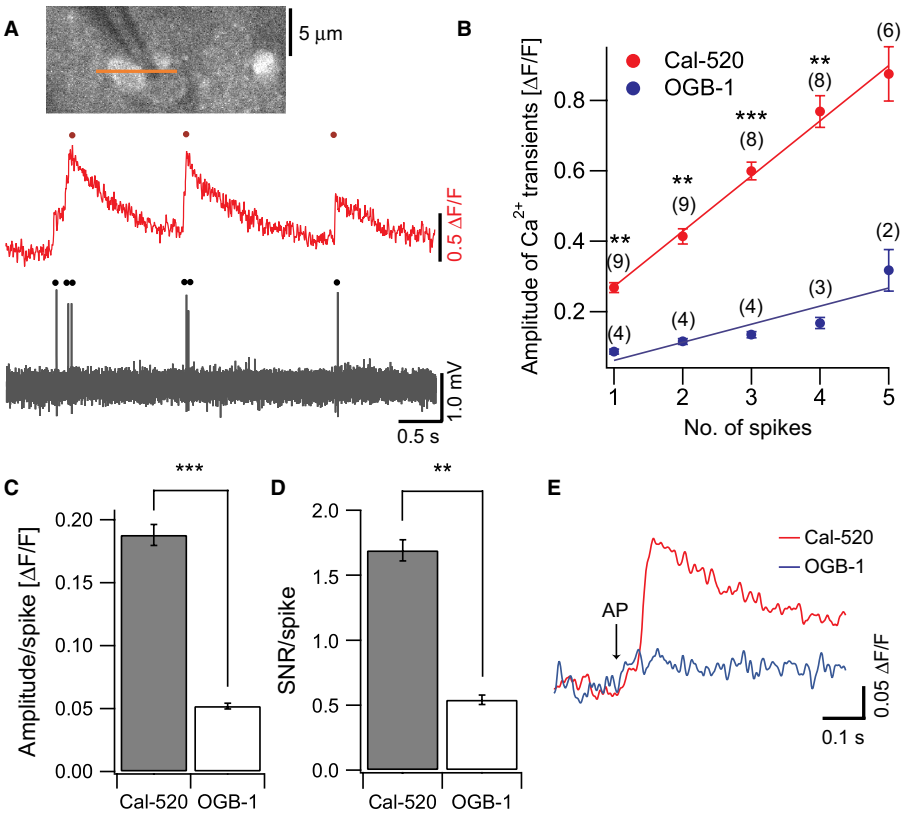

FIG. 5. Simultaneous recordings of calcium transients and APs in neocortical neurons *in vivo*. (A) Representative traces of simultaneous recordings of calcium transients (upper) and APs (lower). (B) Peak amplitude of calcium transients increased proportionally with the number of APs. Lines show linear fit to the data (Spearman's ρ, 0.997 for Cal-520 and 0.939 for OGB-1). Values given in parentheses indicate the number of cells. The data for one and two spikes for OGB-1 were obtained by spike-triggered average of fluorescence traces. $^{**}P < 0.003$, $^{***}P < 0.0001$. (C) The amplitude and (D) SNR of calcium transients normalised by the number of APs ($n = 9$ cells for Cal-520, $n = 4$ cells for OGB-1). $^{**}P = 0.002$, $^{***}P < 0.001$. (E) Average traces of calcium transients in response to a single AP measured with Cal-520 (red, $n = 9$ cells) or OGB-1 (blue, $n = 4$ cells). Note that Cal-520 could clearly detect calcium signals by single APs.

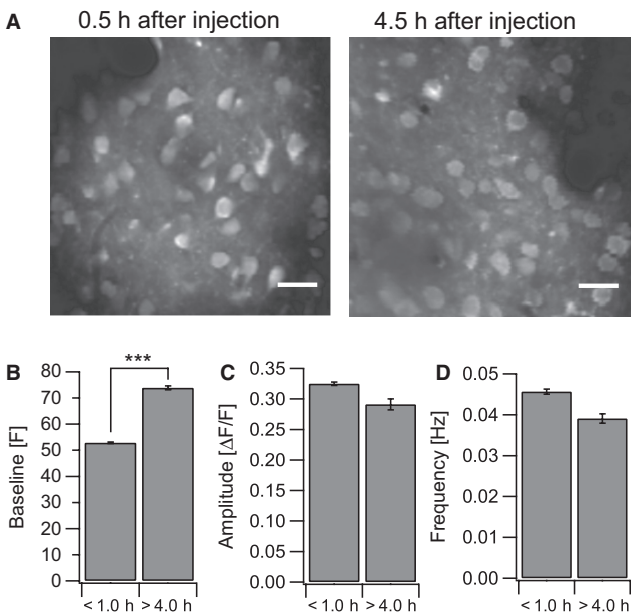

FIG. 6. Time course of the change in fluorescence signals by Cal-520. (A) Fluorescence images of layer 2/3 pyramidal neurons in the barrel cortex recorded at 0.5 h (left) and 4.5 h (right) after the injection of Cal-520. Scale bars, 20 μm. Bar graphs showing the mean baseline fluorescence (B), amplitude (C) and frequency (D) of calcium transients by Cal-520 recorded within 1.0 h or more than 4 h after the injection. $^{***}P = 0.00002$.

transients was significantly larger in cells labeled with Cal-520 than those labeled with OGB-1 (1.788 ± 0.500 and 0.275 ± 0.020 ΔF/F, respectively, $P = 0.04$) (Fig. 7D), which resulted in much higher SNRs (87.834 ± 13.42 for Cal-520 and 18.001 ± 2.772 for OGB-1, respectively, $P = 0.0004$) (Fig. 7E). The mean values of the 10–90 rise time were similar between the two indicators (0.013 ± 0.001 s for Cal-520 and 0.014 ± 0.001 s for OGB-1, $P = 0.364$) (Fig. 7F), whereas the calcium transients measured with Cal-520 had shorter decay times than those measured with OGB-1 (0.011 ± 0.004 and 0.174 ± 0.083 s for Cal-520, 0.044 ± 0.007 and 0.918 ± 0.110 s for OGB-1, $P = 0.0005$ and $P = 0.006$, respectively) (Fig. 7G). These results indicate that Cal-520 can elicit calcium signals with higher SNRs and better temporal resolution than OGB-1 and is therefore suitable for calcium imaging of Purkinje cells *in vivo*.

Discussion

In this article, we demonstrated that a new fluorescent calcium indicator dye, Cal-520, is highly sensitive and has an excellent SNR, which is sufficient to detect single APs both *in vitro* and *in vivo*. The amplitude of calcium transients is linearly correlated with the number of APs, and individual APs in a train up to 10 Hz can be resolved. These properties enable reliable high-resolution optical recordings of spatiotemporal activity patterns of neural circuits in the intact brain.

Calcium imaging of the spiking activity of single neurons *in vitro* and that of neuronal populations *in vivo* clearly showed that Cal-520

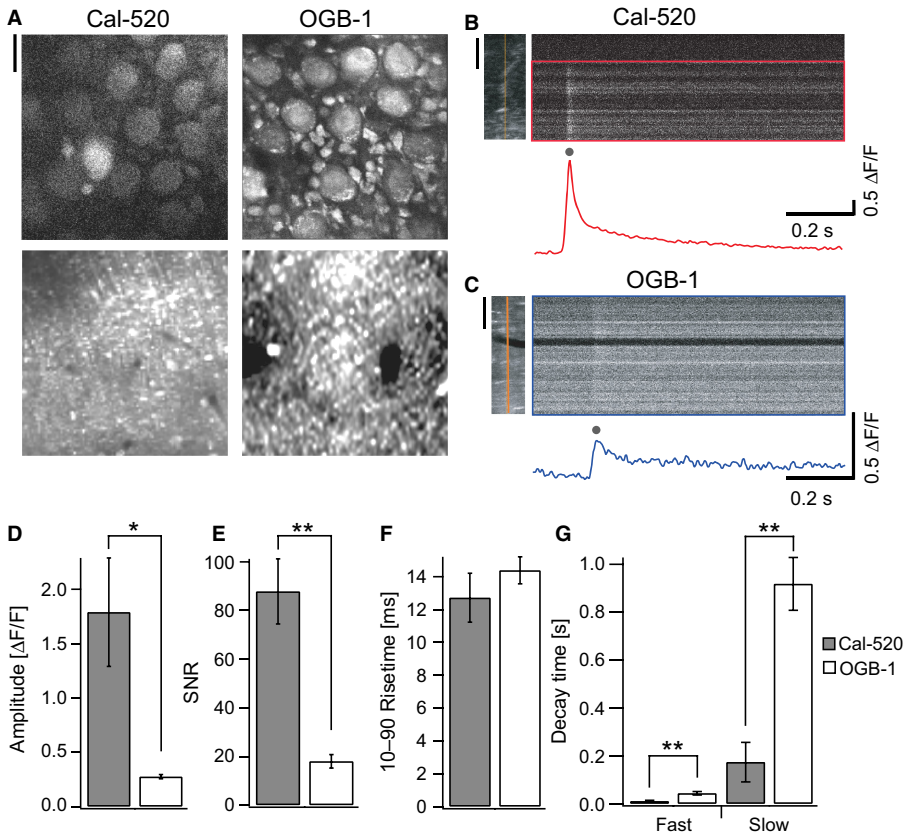

FIG. 7. *In vivo* two-photon calcium imaging of cerebellar Purkinje cell dendrites. (A) Fluorescence images showing the Purkinje cell layer (upper) and molecular layer (lower) of the cerebellar cortex labeled with Cal-520 (left) or OGB-1 (right). Scale bar, 20 μm. (B and C) High-speed linescan imaging of calcium transients in Purkinje cell dendrites. Upper left: images showing dendritic branches of Purkinje cells, ~140 μm from the soma, labeled with Cal-520 (B) or OGB-1 (C). Upper right: representative images obtained by high-speed linescan at the position indicated by the orange lines in the upper left panels. Scale bars, 20 μm. Lower traces show the spontaneous calcium transients. Gray dots indicate calcium transients detected from the baseline noise. (D–G) Bar graphs showing the properties of calcium transients measured with Cal-520 (filled columns) or OGB-1 (open columns). Cal-520 showed larger mean amplitude of calcium transients than OGB-1 (D), resulting in higher SNR (E). 10–90 rise times were indistinguishable between Cal-520 and OGB-1 (F). Both fast and slow decay times were shorter in dendrites labeled with Cal-520 than those with OGB-1 (G). Five cells in four mice for Cal-520 and six cells in two mice for OGB-1. $*P < 0.05$, $**P < 0.01$. Error bars indicate SEM.

has better sensitivity and SNR than OGB-1. In fact, the number of active neurons observed in the barrel cortex *in vivo* was fourfold larger by Cal-520 than by OGB-1, indicating that Cal-520 is especially useful for monitoring the activity of neurons with very low firing rates, such as layer 2/3 neurons of the barrel cortex. The better signal detection performance of Cal-520 has been shown to be attributable to larger signal changes and higher SNR in response to neural activity. Although another fluorescent indicator, Fluo-4 acetoxymethyl ester, can resolve single APs in the neocortex *in vivo* (Sato *et al.*, 2007), its signal in neurons fades rather quickly (Golshani *et al.*, 2009) and staining tends to be biased toward glia (Hirase *et al.*, 2004; Kuga *et al.*, 2011). Cal-520 AM stays in neurons for several hours after injection and shows a similar fluorescence change, thus it has clear advantages for the long-duration imaging of neural activity. The kinetic properties of somatic calcium signals by Cal-520 were similar to those by OGB-1, but showed faster decay than OGB-1 in dendrites. These results indicate that the somatic calcium changes are limited by the small surface-to-volume ratio, even though the kinetics of Cal-520 itself is better than that of OGB-1. In addition, we noticed that the specificity of neuron labeling by multi-cell bolus loading of the acetoxymethyl ester was higher for Cal-520 [compare the images in Figs 2A and B, and 6A; however, in some experiments, we could also observe slow calcium transients presumably due to signals in cortical astrocytes (Hirase *et al.*, 2004; Nimmerjahn *et al.*, 2004)]. Although the mechanism of this labeling specificity is unknown, this property might also contribute to better SNRs in population calcium imaging *in vivo*. In contrast, one disadvantage of Cal-520 was that the spread of dye solution was smaller than that of OGB-1 (data not shown) and thus multiple injections might be required for the imaging of large areas.

Recently, genetically-encoded calcium indicators have been extensively developed and their sensitivity has been improved comparable to that of synthetic calcium indicators (Horikawa *et al.*, 2010; Akerboom *et al.*, 2012; Ohkura *et al.*, 2012a,b; Chen *et al.*, 2013). Genetically-encoded calcium indicators have several advantages, e.g. cell-type specificity and capability of repeated chronic imaging from the same neurons. However, synthetic indicators are still convenient for acute experiments, such that the high sensitivity and SNR can be achieved without the prior introduction of transgenes by viral transfection or use of transgenic animals. Therefore, Cal-520 is a useful tool to provide high sensitivity and better temporal resolution for both *in vitro* and *in vivo* calcium imaging experiments.

Acknowledgements

We thank Dr Taro Ishikawa for providing the analysis program (TaroTools for Igor Pro) and members of the laboratory of M.K. for discussion. This work was supported by Grants-in-aid for Scientific Research (23115504,

25560432, 25115705 and 25290003 to K.K.; 21220006 and 25000015 to M.K.), the Strategic Research Program for Brain Sciences (Development of Biomarker Candidates for Social Behavior), the Global COE Program (Integrative Life Science Based on the Study of Biosignaling Mechanisms) from MEXT Japan, and the PRESTO program from JST (to K. K.).

Abbreviations

AP, action potential; Cal-520 AM, Cal-520 acetoxymethyl ester; OGB-1, Oregon Green 488 BAPTA-1; OGB-1 AM, Oregon Green 488 BAPTA-1 acetoxymethyl ester; SNR, signal-to-noise ratio.

References

Akerboom, J., Chen, T.W., Wardill, T.J., Tian, L., Marvin, J.S., Mutlu, S., Calderon, N.C., Esposti, F., Borghuis, B.G., Sun, X.R., Gordus, A., Orger, M.B., Portugues, R., Engert, F., Macklin, J.J., Filosa, A., Aggarwal, A., Kerr, R.A., Takagi, R., Kracun, S., Shigetomi, E., Khakh, B.S., Baier, H., Lagnado, L., Wang, S.S., Bargmann, C.I., Kimmel, B.E., Jayaraman, V., Svoboda, K., Kim, D.S., Schreiter, E.R. & Looger, L.L. (2012) Optimization of a GCaMP calcium indicator for neural activity imaging. *J. Neurosci.*, **32**, 13819–13840.

Chen, X., Leischner, U., Rochefort, N.L., Nelken, I. & Konnerth, A. (2011) Functional mapping of single spines in cortical neurons *in vivo*. *Nature*, **475**, 501–505.

Chen, T.W., Wardill, T.J., Sun, Y., Pulver, S.R., Renninger, S.L., Baohan, A., Schreiter, E.R., Kerr, R.A., Orger, M.B., Jayaraman, V., Looger, L.L., Svoboda, K. & Kim, D.S. (2013) Ultrasensitive fluorescent proteins for imaging neuronal activity. *Nature*, **499**, 295–300.

Eilers, J., Augustine, G.J. & Konnerth, A. (1995) Subthreshold synaptic Ca^{2+} signalling in fine dendrites and spines of cerebellar Purkinje neurons. *Nature*, **373**, 155–158.

Finch, E.A. & Augustine, G.J. (1998) Local calcium signalling by inositol-1,4,5-trisphosphate in Purkinje cell dendrites. *Nature*, **396**, 753–756.

Golshani, P., Goncalves, J.T., Khoshkhoo, S., Mostany, R., Smirnakis, S. & Portera-Cailliau, C. (2009) Internally mediated developmental desynchronization of neocortical network activity. *J. Neurosci.*, **29**, 10890–10899.

Grewe, B.F. & Helmchen, F. (2009) Optical probing of neuronal ensemble activity. *Curr. Opin. Neurobiol.*, **19**, 520–529.

Grewe, B.F., Langer, D., Kasper, H., Kampa, B.M. & Helmchen, F. (2010) High-speed in vivo calcium imaging reveals neuronal network activity with near-millisecond precision. *Nat. Methods*, **7**, 399–405.

Grienberger, C. & Konnerth, A. (2012) Imaging calcium in neurons. *Neuron*, **73**, 862–885.

Grynkiewicz, G., Poenie, M. & Tsien, R.Y. (1985) A new generation of Ca^{2+} indicators with greatly improved fluorescence properties. *J. Biol. Chem.*, **260**, 3440–3450.

Hashizume, M., Miyazaki, T., Sakimura, K., Watanabe, M., Kitamura, K. & Kano, M. (2013) Disruption of cerebellar microzonal organization in GluD2 (GluRδ2) knockout mouse. *Front. Neural Circuits*, **7**, 130.

Hirase, H., Qian, L., Bartho, P. & Buzsaki, G. (2004) Calcium dynamics of cortical astrocytic networks *in vivo*. *PLoS Biol.*, **2**, E96.

Horikawa, K., Yamada, Y., Matsuda, T., Kobayashi, K., Hashimoto, M., Matsu-ura, T., Miyawaki, A., Michikawa, T., Mikoshiba, K. & Nagai, T. (2010) Spontaneous network activity visualized by ultrasensitive Ca^{2+} indicators, yellow Cameleon-Nano. *Nat. Methods*, **7**, 729–732.

Ikegaya, Y., Le Bon-Jego, M. & Yuste, R. (2005) Large-scale imaging of cortical network activity with calcium indicators. *Neurosci. Res.*, **52**, 132–138.

Jia, H., Rochefort, N.L., Chen, X. & Konnerth, A. (2010) Dendritic organization of sensory input to cortical neurons *in vivo*. *Nature*, **464**, 1307–1312.

Kerr, J.N., Greenberg, D. & Helmchen, F. (2005) Imaging input and output of neocortical networks *in vivo*. *Proc. Natl. Acad. Sci. USA*, **102**, 14063–14068.

Kerr, J.N., de Kock, C.P., Greenberg, D.S., Bruno, R.M., Sakmann, B. & Helmchen, F. (2007) Spatial organization of neuronal population responses in layer 2/3 of rat barrel cortex. *J. Neurosci.*, **27**, 13316–13328.

Kitamura, K. & Häusser, M. (2011) Dendritic calcium signaling triggered by spontaneous and sensory-evoked climbing fiber input to cerebellar Purkinje cells *in vivo*. *J. Neurosci.*, **31**, 10847–10858.

Kuga, N., Sasaki, T., Takahara, Y., Matsuki, N. & Ikegaya, Y. (2011) Large-scale calcium waves traveling through astrocytic networks *in vivo*. *J. Neurosci.*, **31**, 2607–2614.

Miyakawa, H., Ross, W.N., Jaffe, D., Callaway, J.C., Lasser-Ross, N., Lisman, J.E. & Johnston, D. (1992) Synaptically activated increases in Ca^{2+} concentration in hippocampal CA1 pyramidal cells are primarily due to voltage-gated Ca^{2+} channels. *Neuron*, **9**, 1163–1173.

Mukamel, E.A., Nimmerjahn, A. & Schnitzer, M.J. (2009) Automated analysis of cellular signals from large-scale calcium imaging data. *Neuron*, **63**, 747–760.

Nimmerjahn, A., Kirchhoff, F., Kerr, J.N. & Helmchen, F. (2004) Sulforhodamine 101 as a specific marker of astroglia in the neocortex *in vivo*. *Nat. Methods*, **1**, 31–37.

Ohki, K., Chung, S., Ch'ng, Y.H., Kara, P. & Reid, R.C. (2005) Functional imaging with cellular resolution reveals precise micro-architecture in visual cortex. *Nature*, **433**, 597–603.

Ohkura, M., Sasaki, T., Kobayashi, C., Ikegaya, Y. & Nakai, J. (2012a) An improved genetically encoded red fluorescent Ca^{2+} indicator for detecting optically evoked action potentials. *PLoS ONE*, **7**, e39933.

Ohkura, M., Sasaki, T., Sadakari, J., Gengyo-Ando, K., Kagawa-Nagamura, Y., Kobayashi, C., Ikegaya, Y. & Nakai, J. (2012b) Genetically encoded green fluorescent Ca^{2+} indicators with improved detectability for neuronal Ca^{2+} signals. *PLoS ONE*, **7**, e51286.

Ozden, I., Sullivan, M.R., Lee, H.M. & Wang, S.S. (2009) Reliable coding emerges from coactivation of climbing fibers in microbands of cerebellar Purkinje neurons. *J. Neurosci.*, **29**, 10463–10473.

Pologruto, T.A., Sabatini, B.L. & Svoboda, K. (2003) ScanImage: flexible software for operating laser scanning microscopes. *Biomed. Eng. Online*, **2**, 13.

Regehr, W.G., Connor, J.A. & Tank, D.W. (1989) Optical imaging of calcium accumulation in hippocampal pyramidal cells during synaptic activation. *Nature*, **341**, 533–536.

Rochefort, N.L., Narushima, M., Grienberger, C., Marandi, N., Hill, D.N. & Konnerth, A. (2011) Development of direction selectivity in mouse cortical neurons. *Neuron*, **71**, 425–432.

Sato, T.R., Gray, N.W., Mainen, Z.F. & Svoboda, K. (2007) The functional microarchitecture of the mouse barrel cortex. *PLoS Biol.*, **5**, e189.

Schultz, S.R., Kitamura, K., Post-Uiterweer, A., Krupic, J. & Häusser, M. (2009) Spatial pattern coding of sensory information by climbing fiber-evoked calcium signals in networks of neighboring cerebellar Purkinje cells. *J. Neurosci.*, **29**, 8005–8015.

Smith, S.L. & Häusser, M. (2010) Parallel processing of visual space by neighboring neurons in mouse visual cortex. *Nat. Neurosci.*, **13**, 1144–1149.

Sohya, K., Kameyama, K., Yanagawa, Y., Obata, K. & Tsumoto, T. (2007) GABAergic neurons are less selective to stimulus orientation than excitatory neurons in layer II/III of visual cortex, as revealed by *in vivo* functional Ca^{2+} imaging in transgenic mice. *J. Neurosci.*, **27**, 2145–2149.

Stosiek, C., Garaschuk, O., Holthoff, K. & Konnerth, A. (2003) *In vivo* two-photon calcium imaging of neuronal networks. *Proc. Natl. Acad. Sci. USA*, **100**, 7319–7324.

Sullivan, M.R., Nimmerjahn, A., Sarkisov, D.V., Helmchen, F. & Wang, S.S. (2005) *In vivo* calcium imaging of circuit activity in cerebellar cortex. *J. Neurophysiol.*, **94**, 1636–1644.

Svoboda, K., Tank, D.W. & Denk, W. (1996) Direct measurement of coupling between dendritic spines and shafts. *Science*, **272**, 716–719.

Svoboda, K., Denk, W., Kleinfeld, D. & Tank, D.W. (1997) *In vivo* dendritic calcium dynamics in neocortical pyramidal neurons. *Nature*, **385**, 161–165.

Takahashi, N., Kitamura, K., Matsuo, N., Mayford, M., Kano, M., Matsuki, N. & Ikegaya, Y. (2012) Locally synchronized synaptic inputs. *Science*, **335**, 353–356.

Tsien, R.Y. (1981) A non-disruptive technique for loading calcium buffers and indicators into cells. *Nature*, **290**, 527–528.

Waters, J., Larkum, M., Sakmann, B. & Helmchen, F. (2003) Supralinear Ca^{2+} influx into dendritic tufts of layer 2/3 neocortical pyramidal neurons *in vitro* and *in vivo*. *J. Neurosci.*, **23**, 8558–8567.

Wimmer, V.C., Nevian, T. & Kuner, T. (2004) Targeted *in vivo* expression of proteins in the calyx of Held. *Pflug. Arch.*, **449**, 319–333.

Yasuda, R., Nimchinsky, E.A., Scheuss, V., Pologruto, T.A., Oertner, T.G., Sabatini, B.L. & Svoboda, K. (2004) Imaging calcium concentration dynamics in small neuronal compartments. *Sci. STKE*, **2004**, l5.

Yuste, R. & Denk, W. (1995) Dendritic spines as basic functional units of neuronal integration. *Nature*, **375**, 682–684.

Yuste, R. & Katz, L.C. (1991) Control of postsynaptic Ca^{2+} influx in developing neocortex by excitatory and inhibitory neurotransmitters. *Neuron*, **6**, 333–344.

Yuste, R., MacLean, J., Vogelstein, J. & Paninski, L. (2011) Imaging action potentials with calcium indicators. *Cold Spring Harb. Protoc.*, **2011**, 985–989.